Electronic Supplementary Information (ESI) for

Metal carbide/Ni hybrids for high-performance electromagnetic absorption and absorption-based electromagnetic interference shielding

Qindong Xie,[†] Zhiyang Yan,[‡] Feng Qin,*,[‡] Le Wang,[†] Lin Mei,[†] Yanpei Zhang,[†] Zhongke

Wang,[†] Guangtao Zhao,[†] and Ruibin Jiang*,[†]

[†]Shaanxi Key Laboratory for Advanced Energy Devices, Shaanxi Engineering Lab for

Advanced Energy Technology, School of Materials Science and Engineering, Shaanxi

Normal University, Xi'an 710119, China

[‡]Key Laboratory of Science and Technology on Complex Electromagnetic Environment,

China Academy of Engineering Physics, Mianyang 621900, China

Contents

1. Experimental Details

1.1. Materials

Lithium fluoride (LiF, 98.5%, Aladdin), hydrochloric acid (HCl, 36-38%, Sinopharm Chemical Reagent Co., Ltd.), hydrazine monohydrate ($N_2H_4 \cdot H_2O$, 50%, Aladdin), polyvinyl pyrrolidone (PVP, MW ~29000, Aladdin), Ti_3AlC_2 Max phase (400 mesh, <30.8 μm, Laizhou Kai Kai Ceramic Materials Co., Ltd.), nickel chloride hexahydrate ($NiCl_2 \cdot 6H_2O$, 98%, Aladdin), ammonia solution ($NH_3 \cdot H_2O$, 25%~28%, Sinopharm Chemical Reagent Co., Ltd.), durapore filter membrane (polyvinyldifluoride (PVDF), pore size 0.1 μm). All chemical reagents were used directly from commercial suppliers without further processing.

1.2. Preparation of $Ti_3C_2T_x$ MXene

$Ti_3C_2T_X$ was synthesized by etching Ti_3AlC_2 phase (<30.8 μm) with LiF/HCl.[1] Specifically, LiF (1 g) and HCl (20 mL, 9 M) were first mixed by stirring in a Teflon vessel. Ti_3AlC_2 powder (1 g) was then slowly added into the mixture. The obtained dispersion was kept stirring for 24 h at 35 °C. After the reaction, the resultant was collected by centrifugation at 3500 rpm for 5 min and washed repeatedly with deionized water. Finally, the homogeneous delaminated $Ti_3C_2T_x$ supernatant was obtained by sonication for 1 h under Ar flow, followed by centrifugation at 3500 rpm for 1 h. The resulting supernatant has $Ti_3C_2T_x$ concentration of 2 mg/mL.

1.3. Preparation of $Ti_3C_2T_x$/Ni Hybrid Nanostructures

The $Ti_3C_2T_x$/Ni hybrid nanostructures were prepared through two steps. In the first step, $Ti_3C_2T_x$ adsorbed Ni^{2+} was obtained. Specifically, different amounts of aqueous $NiCl_2 \cdot 6H_2O$ solution (10 mg/mL) were added into 91.7 mL of $Ti_3C_2T_x$ (2 mg/mL), followed by the addition of PVP. To obtain Ni contents of 1 wt.%, 5 wt.%, and 10 wt.% in the precursors, the addition amounts of $NiCl_2 \cdot 6H_2O$ solution were 0.83 mL, 4.15 mL, and 8.3 mL, respectively,

and the corresponding PVP amounts were 10 mg, 30 mg, and 50 mg, respectively. After the addition of $NiCl_2 \cdot 6H_2O$ solution and PVP, deionized water was added to adjust the total volume of $Ti_3C_2T_x$-Ni^{2+} mixed solutions to 100 mL. The resultant mixture was then stirred at room temperature for 24 h to adsorb Ni^{2+} sufficiently. In the second step, the mixed solution was first heated to 60 °C. Hydrazine monohydrate ($N_2H_4 \cdot H_2O$) was then introduced as the reducing agent. After 5 min, 0.5 mL of $NH_3 \cdot H_2O$ was added. The mixture solution was kept at 60 °C for 5 hours to produce $Ti_3C_2T_x$/Ni hybrid nanostructures. The samples with Ni contents of 1 wt.%, 5 wt.%, and 10 wt.% were named as $Ti_3C_2T_x$/Ni-1, $Ti_3C_2T_x$/Ni-5, and $Ti_3C_2T_x$/Ni-10, respectively.

1.4. Fabrication of Free-Standing $Ti_3C_2T_x$/Ni Film

$Ti_3C_2T_x$ and $Ti_3C_2T_x$/Ni films were fabricated through vacuum-assisted filtration with Durapore filter membrane (PVDF, pore size 0.1 μm). Specifically, different amounts of sample dispersions (5 mg/mL) were filtered until dry for 24–72 h at room temperature to fabricate films with different thickness. Free-standing films were obtained through peeling the film off the filter membrane after the films were dried at room temperature. To study the absorption of different samples toward electromagnetic waves, paraffin-based composites were prepared with different $Ti_3C_2T_x$/Ni hybrid nanostructures.

1.5. Characterization

The morphologies of samples were characterized by SEM (SU8220, Hitachi, 5 kV), TEM (JEM-2100, JEOL, 200 kV) and AFM (Dimension Icon Bruker). HRTEM imaging was carried out on a JEOL JEM-2100 operating at 200 kV. EDX elemental maps were obtained on an FEI Tecnai F20 microscope equipped with an Oxford EDX analysis system. XRD patterns were conducted on a Rigaku Smartlab (XRD; Rigaku, Miniflex600) diffractometer with Cu Kα (λ = 1.5406 Å) radiation. The chemical bonding information was obtained with X-ray

photoelectron spectra (XPS) (Axis Ultra, Kratos Analytical Ltd, Japan) equipped with a monochromatized Al Kα X-ray source (1486.6 eV). The binding energy was corrected by the C 1s line at 284.6 eV. Fourier transform infrared spectroscopy (FTIR) were recorded in the range of 400−4000 cm^{-1} using a semiconductor parameter analyzer (spectrum two, PerkinElmer, USA). The conductivity of the prepared composites was measured by a four-point probe instrument (RTS-9, Guangzhou, China). EDX for identifying the element contents was carried out on SEM (SU8020, Hitachi, 15 kV) with Horiba EDX Spectrometer.

1.6. Electromagnetic Absorption and Electromagnetic Interference Shielding Measurements

Paraffin-based composites containing different nanostructures were pressed into a toroidal shape with an inner diameter of 3.00 mm and an outer diameter of 7.00 mm. The dielectric constant and magnetic permeability were measured using two-port vector network analyzer (Rohde & Schwarz ZVB 20, Germany) over the frequency of 2−18 GHz.

Electromagnetic interference shielding of samples was measured using waveguide method by a vector network analyzer (VNA) (Agilent, E8363B, USA) in the X-band. The samples for the S-parameter measurements have diameters of 45 mm. The reflection coefficient R, transmission coefficient T, and absorption coefficient A were determined from S parameters as follows: $T = |S_{12}|^2 = |S_{12}|^2$, $R = |S_{11}|^2 = |S_{22}|^2$, and $A = 1 - R - T$, where S_{11}, S_{22}, S_{12}, and S_{21} are input reflection, output reflection, reverse transmission, and forward transmission, respectively.

2. Supporting Figures and Tables
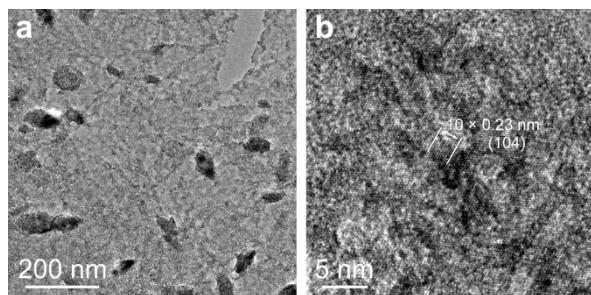
Figure S1. a) Large magnification TEM image of $Ti_3C_2T_x$ nanosheet. b) HRTEM taken on a nanoparticle on $Ti_3C_2T_x$ nanosheet. The lattice fringes indicate that the nanoparticle is $Ti_3C_2T_x$.
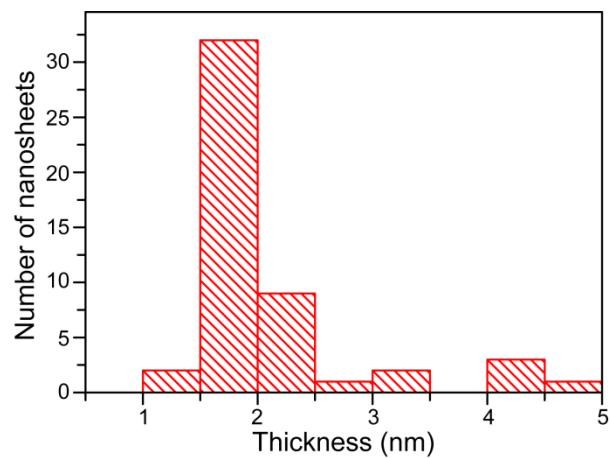
Figure S2. Thickness distribution of MXene nanosheets. It can be found that most of MXene nanosheets have thickness in the range of 1.5–2 nm. The thicknesses are obtained from AFM image.
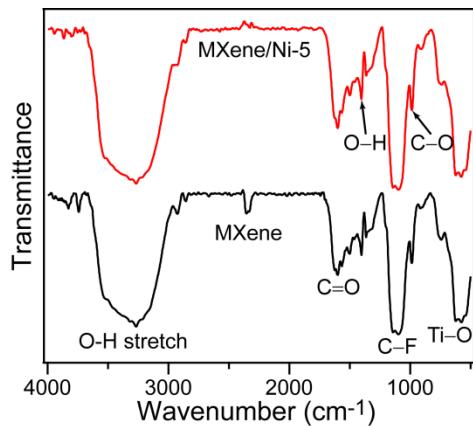
Figure S3. FTIR spectra of $Ti_3C_2T_x$ MXene and $Ti_3C_2T_x$ MXene/Ni-5.
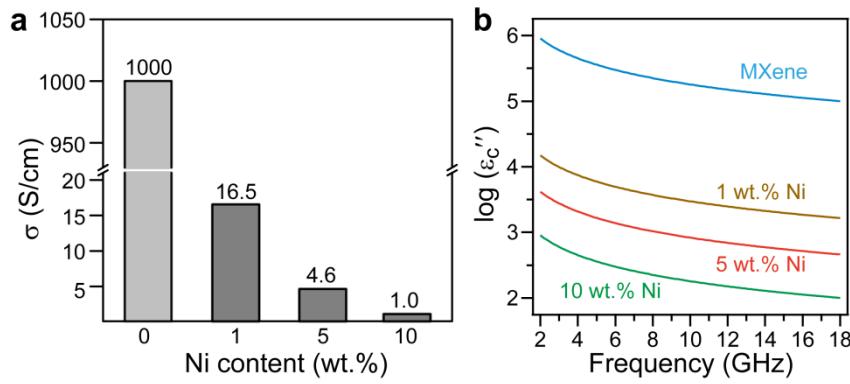
Figure S4. a) Electrical conductivity of $Ti_3C_2T_x$ MXene and $Ti_3C_2T_x$ MXene/Ni hybrid nanostructure with different Ni loading. b) Conductance loss of different samples.
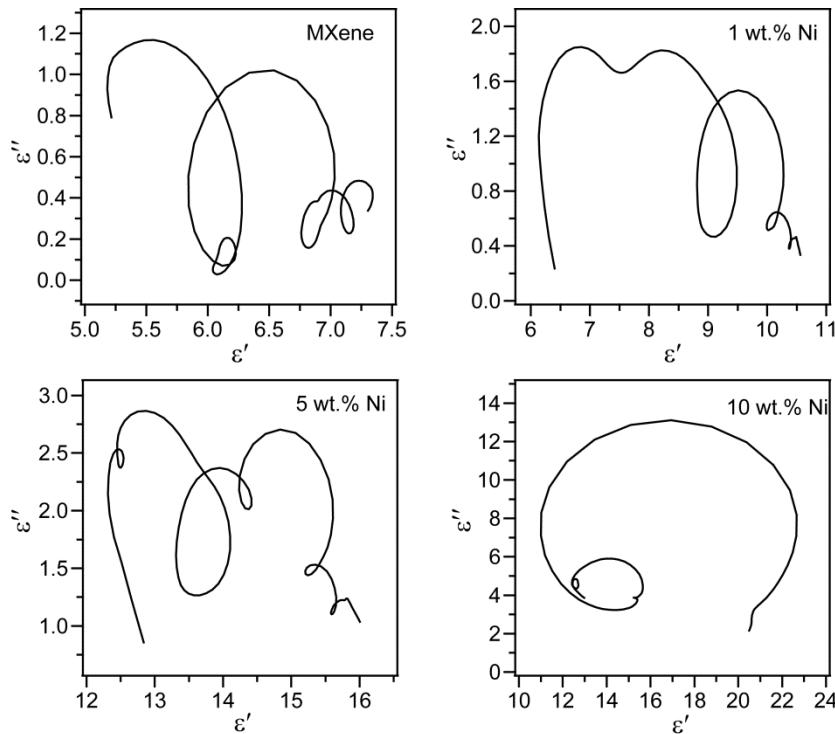
Figure S5. Cole-Cole figure of different samples.
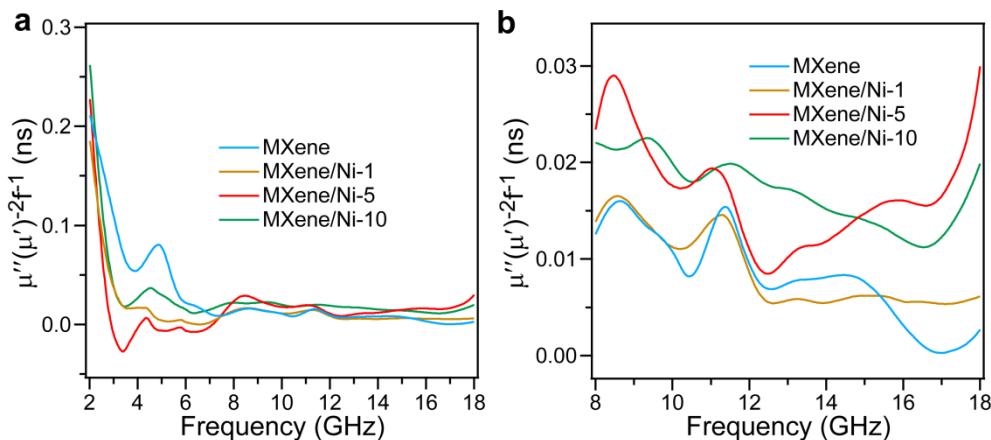
Figure S6. Values of $\mu''(\mu')^{-2}f^{1}$ for the composites vs. frequency. a) Values of $\mu''(\mu')^{-2}f^{1}$ in the frequency range of 2−18 GHz. b) Enlarged plots in the frequency range of 8−18 GHz.
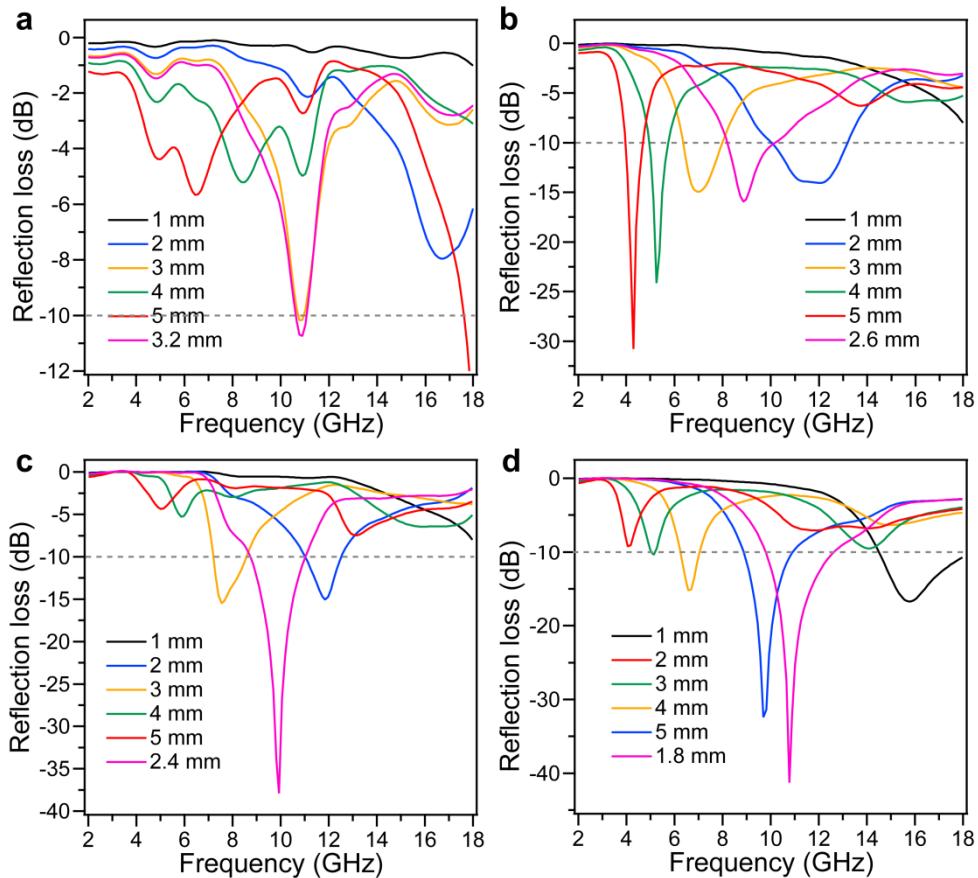
Figure S7. Reflection loss at different thicknesses. a) $Ti_3C_2T_x$ MXene. b–d) $Ti_3C_2T_x$ MXene/Ni-1, MXene/Ni-5, and MXene/Ni-10, respectively. The gray dashed lines indicate the RL value of -10 dB.
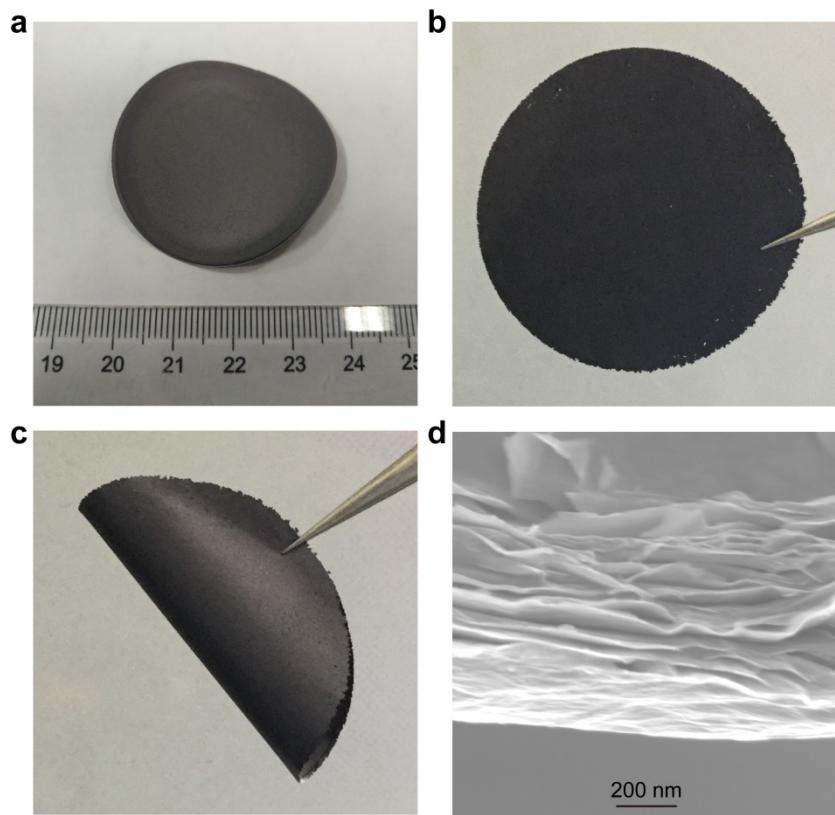
Figure S8. Film of $Ti_3C_2T_x$ MXene/Ni-5. a) Photograph of the film on filter paper. b,c) Photograph of the film lifted off the filter paper. It can be found that the film is relatively flexible. d) SEM image of the cross section of the film.
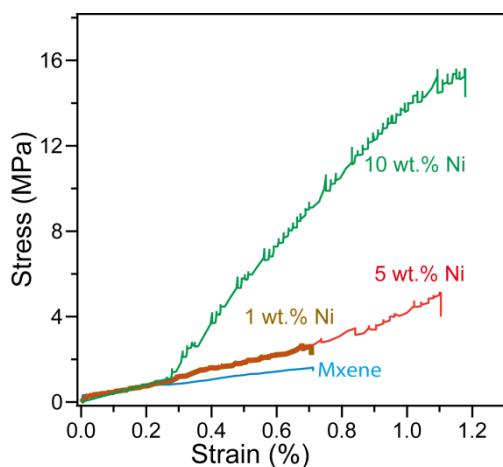
Figure S9. Tensile stress-strain curves of $Ti_3C_2T_x$ MXene and $Ti_3C_2T_x$ MXene/Ni hybrid nanostructure with different amounts of Ni loading. The strain rate is 1.5 mm/min. The film thicknesses are 50 μm.

Table S1. Relationship between shielding effectiveness (dB) and shielding efficiency (%).

Shielding Effectiveness (dB)	Shielding Efficiency (%)
0	0
10	90
20	99
30	99.9
40	99.99
50	99.999
60	99.9999
62	99.99994

Table S2. EMI shielding materials of various materials

| Materials type	Filler	Filler (wt.%)	Matrix	Thickness (mm)	EMI SE (dB)	Ref.
MXene film	$Ti_3C_2T_X$	87.5	Pedot:PSS	0.0111	42.1	2
	$Ti_3C_2T_X$	90	CNF	0.047	22	3
	$Ti_3C_2T_X$	/	textile	0.43	41	4
	$Ti_3C_2T_X$	90	SA	0.008	57	5
	Ti_2CT_X	30	wax	0.8	70	6
	$Ti_3C_2T_X$	1.9 vol.%	PS	2.0	62	7
	$MWCNT/Ti_3C_2T_X$	/	PVA&PSS	0.00017	2.8	8
	$SWCNT/Ti_3C_2T_X$	/	PVA&PSS	0.000207	3.34	8
MXene foam	$Ti_3C_2T_X$	/	/	0.06	71	9
	$Ti_3C_2T_X$	90	CA	0.026	54.3	10
	Ti_2CT_X	7.6 vol.%	PVA	0.1	47.7	11
Metal film	Co	60	PVDF/CNT	0.3	35.3	12
	TiN_X	/	/	0.00147	>20	13
	Ni	20	PVDF	0.3	27.6	14
	Ag	7.75	PLA	2.7	60.4	15
	Ni-CF	/	PC	0.31	72.7	16
	Ag	5.46	PU	0.36	106	17
	Ag/ZnO	5.7 vol%	WPU	0.5	87.2	18
	Ni/GMP	30	wax	0.7	40	19
Carbon film	rGO	7	PS	2.5	45.1	20
	rGO	/	/	0.014	73.7	22

	graphene	/	/	0.01	25	23
	LG paper	/	/	0.0125	52.5	24
	MWCNT	80	PU	2.3	46.7	25
	graphene	2 vol.%	B_4C	1.5	35	26
	CNT	5	PVDF	0.1	22.41	27
	CNT	8	PVDF	0.1	25.02	27
	CNT/graphene	5/10	PVDF	0.1	27.58	27
	rGO	/	$TiO_2/SiO_2/PPy$	0.244	30	28
	graphene	3.07	PDMS	2.0	54	29
	GO/CNT	15	SiCN	2.0	67.2	30
	G/GNT	/	UHMWPE	0.5	31.8	31
Carbon film	graphene	/	/	2.0	48.7	32
	rGo	0.66	epoxy	2.0	33	21
	MWCNT	0.5	epoxy/rubber	2.0	22.9	33
	Ag@C	/	/	3.0	70.1	34
MXene film	Ni	5	$Ti_3C_2T_X$	0.002	22	This work
	Ni	5	$Ti_3C_2T_X$	0.005	32.6	
	Ni	5	$Ti_3C_2T_X$	0.01	41.05	
	Ni	5	$Ti_3C_2T_X$	0.018	48.6	
	Ni	5	$Ti_3C_2T_X$	0.03	52.4	
	Ni	5	$Ti_3C_2T_X$	0.05	62.7	

References:
[1] M. Alhabeb, K. Maleski, B. Anasori, P. Lelyukh, L. Clark, S. Sin, Y. Gogotsi, *Chem. Mater.* **2017**, *29*, 7633.
[2] R. T. Liu, M. Miao, Y. H. Li, J. F. Zhang, S. M. Cao, X. Feng, *ACS Appl. Mater. Interfaces* **2018**, *10*, 44787.
[3] W. T. Cao, F. F. Chen, Y. J. Zhu, Y. G. Zhang, Y. Y. Jiang, M. G. Ma, F. Chen, *ACS Nano* **2018**, *12*, 4583.
[4] Q. W. Wang, H. B. Zhang, J. Liu, S. Zhao, X. Xie, L. X. Liu, R. Yang, N. Koratkar, Z. Z. Yu, *Adv. Funct. Mater.* **2019**, *29*, 1806819.
[5] F. Shahzad, M. Alhabeb, C. B. Hatter, B. Anasori, S. M. Hong, C. M. Koo, Y. Gogotsi, *Science* **2016**, *353*, 1137.
[6] X. Li, X. Yin, S. Liang, M. Li, L. Cheng, L. Zhang, *Carbon* **2019**,*146*, 210.
[7] R. Sun, H. B. Zhang, J. Liu, X. Xie, R. Yang, Y. Li, S. Hong, Z. Z. Yu, *Adv. Funct. Mater.* **2017**, *27*, 1702807.
[8] G. M. Weng, J. Li, M. Alhabeb, C. Karpovich, H. Wang, J. Lipton, K. Maleski, J. Kong, E. Shaulsky, M. Elimelech, Y. Gogotsi, A. D. Taylor, *Adv. Funct. Mater*. **2018**, *28*, 1803360.
[9] J. Liu, H. B. Zhang, R. Sun, Y. Liu, Z. Liu, A. Zhou, Z. Z. Yu, *Adv. Mater.* **2017**, *29*, 1702367.
[10]Z. Zhou, J. Liu, X. Zhang, D. Tian, Z. Zhan, C. Lu, *Adv. Mater. Interfaces* **2019**, 1802040.

[11] H. Xu, X. Yin, X. Li, M. Li, S. Liang, L. Zhang, L. Cheng, *ACS Appl. Mater. Interfaces* **2019**, *11*, 10198.

[12] X. Li, S. Zeng, S. E, L. Liang, Z. Bai, Y. Zhou, B. Zhao, R. Zhang, *ACS Appl. Mater. Interfaces* **2018**, *10*, 40789.

[13] L. Lu, F. Luo, Y. Qing, W. Zhou, D. Zhu, J. Dong, *Appl. Phys. A* **2018,** *124*, 721.

[14] B. Zhao, S. Zeng, X. Li, X. Guo, Z. Bai, B. Fan. R, Zhang, *J. Mater. Chem. C*, **2020**, *8*, 500.

[15] X. Huang, B. Dai, Y. Ren, J. Xu,. P. Zhu, *J. Nanomater.* **2015**, *2015*, 320306.

[16] D. Xing, L. Lu, K. S. Teh, Z. Wan, Y. Xie, Y. Tang, *Carbon* **2018**, *132*, 32.

[17] L. C. Jia, L. Xu, F. Ren, P. G. Ren, D. X. Yan, Z. M. Li, *Carbon* **2019**, 144, 101.

[18] Y. Xu, Y. Yang, D. X. Yan, H. Duan, G. Zhao, Y. Liu, *ACS Appl. Mater. Interfaces* **2018**, *10*, 19143.

[19] H. J. Im, G. H. Jun, D. J. Lee, H. J. Ryu, S. H. Hong, *J. Mater. Chem. C* **2017**, *5*, 6471.

[20] D. X, Yan, H, Pang, B. Li, R. Vajtai, L. Xu, P. G. Ren, J. H. Wang, Z. M. Li, *Adv. Funct. Mater.* **2015**, *25*, 559.

[21] Y. Chen, H. B. Zhang, Y. Yang, M. Wang, A. Cao, Z. Z. Yu, *Adv. Funct. Mater.* **2016**, *26*, 447.

[22] S. Lin, S. Ju, J. Zhang, G. Shi, Y. He, D. Jiang, *RSC Adv.* **2019**, *9*, 1419.

[23] S. Wana, Y. Lia, J. Muc, A. E. Alievc, S. Fang, N. A. Kotovb, L. Jiang, Q. Chenga, R. H. Baughmanc, *Proc. Natl. Acad. Sci. U. S. A.* **2018**, *115*, 5359.

[24] Y. J. Wan, P. L. Zhu, S. H. Yu, R. Sun, C. P. Wong, W. H. Liao, *Carbon* **2017**, *122*, 74.

[25] Z. Zeng, H. Jin, M. Chen, W. Li, L. Zhou, X. Xue, Z. Zhang, *Small* **2017**, *13,* 1701388.

[26] Y. Q. Tan, H. Luo, X. S. Zhou, S. M. Peng, H. B. Zhang, *RSC Adv.* **2018**, *8*, 39314.

[27] B. Zhao, C. Zhao, R. Li, S. M. Hamidinejad, C. B. Park, *ACS Appl. Mater. Interfaces* **2017**, *9*, 20873.

[28] L. Huang, J. Li, Y. Li, X. He, Y. Yuan, *Nanoscale* **2019**, *11*, 8616.

[29] F. Xu, R. Chen, Z. Lin, Y. Qin, Y. Yuan, Y. Li, X. Zhao, M. Yang, X. Sun, S. Wang, Q. Peng, Y. Li, X. He, *ACS Omega* **2018**, *3*, 3599.

[30] X. Liu, Z. Yu, R. Ishikawa, L. Chen, X. Liu, X. Yin, Y. Ikuhara, R.Riedel, *Acta Mater.* **2017**, *130*, 83.

[31] L. C. Jia, D. X. Yan, X. Jiang, H. Pang, J.F. Gao, P. G. Ren, Z. M. Li, *Ind. Eng. Chem. Res.* **2018**, *57*, 11929.

[32] Z. Zeng, Y. Zhang, X. Y. D. Ma, S. I. S. Shahabadi, B. Che, P. Wang, X. Lu, *Carbon* **2018**, *140*, 227.

[33] F. Huang, Y. Wang, P. Wang, H. L. Ma, X. Chen, K. Cao, Y. Pei, J. Peng, J. Lia, M, Zhai, *RSC Adv.* **2018**, *8*, 24236.

[34] Y. J. Wan, P. L. Zhu, S. H. Yu, R. Sun, C. P. Wong, W. H. Liao, *Small* **2018**, *14*, 1800534.